

Photorefractive two-wave mixing in semiconductors of the $\bar{4}3m$ space group in general spatial orientation

H. J. Eichler, Y. Ding, and B. Smandek*

Optical Institute, Technical University of Berlin, Straße des 17. Juni 135, D-10623 Berlin, Germany

(Received 7 September 1993; revised manuscript received 4 April 1995)

The photorefractive two-wave mixing gain coefficient Γ of GaAs:Cr and InP:Fe, cut with different crystallographic orientations, was determined using a cw Nd:YAG (neodymium doped yttrium aluminum garnet) laser at 1064 nm. The polarization and orientation dependence of the gain coefficient Γ are calculated from the pertinent interaction matrix elements. Results are discussed with respect to the contactless determination of crystallographic parameters via the photorefractive effect.

PACS number(s): 42.65.Hw, 42.70.Nq

I. INTRODUCTION

Since the discovery of the photorefractive effect in III-V [1,2] and II-VI [3] compound semiconductors, applications of this effect are considered in information transmission [4] and processing [5], beam cleanup [6], laser system design [7], or characterization of semiconductor materials [8,9] using two-wave mixing (TWM) and four-wave mixing (FWM) schemes. High gain coefficients were recently obtained in GaAs [10] and InP [11,12] and used in self-starting oscillators [13,14], in analogy to earlier experiments with photorefractive oxides.

While there are detailed TWM and FWM studies for "holographically cut" crystals, especially with (110) surfaces [15–18], only a few experiments on commercial wafers [8] or crystals with (100) surfaces were performed. This led partially to erroneous interpretations of the origin of the TWM signal [19]. In order to describe TWM experiments in semiconductor wafers with arbitrary crystal orientation and laser beam polarization, we derive the general orientational dependence of the photorefractive gain. The results are compared with measurements using samples cut in different crystallographic orientations.

II. EXPERIMENTAL ARRANGEMENT

We used a TWM experimental setup to determine the photorefractive gain coefficient Γ with a cw Nd:YAG (YAG denotes yttrium aluminum garnet) laser operating at 1064 nm. The experiment was similar to previous ones reported in Ref. [17]. The orientational dependence was recorded by rotating the sample around the surface normal or the z' axis as indicated in Fig. 1. We denote henceforth the crystallographic system as x - y - z and the laboratory system as x' - y' - z' . The polarization of the pump I_{pump} and signal I_{sig} beams could be varied by $\lambda/2$ waveplates. The typical incident angle was 15° outside the crystal. The pump beam was chopped with 100

Hz. The observed signal after the sample was fed into a lock-in amplifier and recorded by a microcomputer. In the case of a large intensity ratio ($\beta > 100$) between the pump and signal beams the observable gain γ_0 was then related to the gain coefficient Γ via

$$\gamma_0 = \frac{I_{sig}(L)}{I_{sig}(0)} = e^{(\Gamma - \alpha)L}, \quad (1)$$

where L is the length of the sample and α is the absorption coefficient. The change of the signal beam with and without the pump beam was between 0.1% and 1%, depending on the sample thickness.

III. THEORETICAL DESCRIPTION

The interference pattern of the two beams creates a periodic modulation of the density of mobile charges. Diffusion and trapping of the latter result in the creation of periodic space charge layers, thereby a periodically varying field \vec{E} . This changes the electrical permittivity ϵ via the linear electro-optic effect (Pockels effect) and the elasto-optic effect, in which the elastic strain is caused by \vec{E} through the converse piezoelectricity (electrorestriction):

$$(\Delta\epsilon)_{ij} = -\epsilon_0 n^4 (r_{ijk} E_k + p_{ijkl} S_{kl}), \quad (2)$$

where ϵ_0 is the permittivity in vacuum; n is the refractive index of the material; and r_{ijk} is the component of the linear electro-optic tensor; p_{ijkl} is the component of the

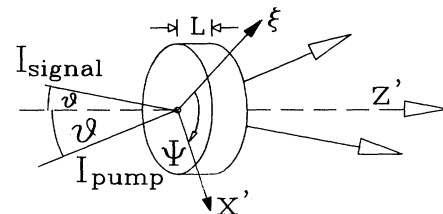


FIG. 1. Experimental setup for two-wave mixing and definition of the laboratory coordinate system.

*Present address: Crystal GmbH, Ostendstrasse 2-14, 12459 Berlin, Germany.

elasto-optic tensor and S_{kl} is the corresponding crystal deformation.

The influence of the second term in Eq. (2) is usually not negligible [20–22] for most ferroelectric oxides and sillenites. For example, the contribution of the elasto-optic effect to the photorefractive effect can be as high as 20–30% in $\text{Bi}_{12}\text{GeO}_{20}$ (BGO) and $\text{Bi}_{12}\text{SiO}_{20}$ (BSO) crystals [19,20]. But in photorefractive semiconductors, although the elasto-optic coefficients are about the same as those of sillenites, the piezoelectric coefficients are much smaller. For example, the piezoelectric coefficient of GaAs is 0.154 C/m² whereas this value of BSO is 1.12 C/m² [20,21]. So the contribution of the piezoelectricity in semiconductors, if any, can be estimated to be smaller than 5%. In the following discussion, we neglect this contribution, i.e., the second term in the parentheses in Eq. (2).

In the $\bar{4}3m$ space group six components of the 27-component tensor $[r_{ijk}]$ are identical and denoted by r_{41} . The other components have zero value [23]. This results in

$$[(\Delta\epsilon)_{ij}] = -\epsilon_0 n^4 r_{41} \begin{pmatrix} 0 & E_z & E_y \\ E_z & 0 & E_x \\ E_y & E_x & 0 \end{pmatrix}, \quad (3)$$

where x , y , and z indicate the crystal axes. Equation (3) represents the orientational dependence of the magnitude of the refractive index grating.

Using Eq. (3), the electromagnetic wave equation is then solved with the slowly varying envelope approximation and neglecting the sample absorption [24]. In the case of small depletion of the pump beam, less than 10^{-4} in our case, and $\pi/2$ phase shift between the refractive index grating and the intensity grating, wave propagation is described by the matrix equation

$$\frac{\partial}{\partial z'} \begin{pmatrix} B_s \\ B_p \end{pmatrix} = \frac{\lambda \omega^2 \mu \epsilon_0}{4\pi n \cos \theta} \begin{pmatrix} \Gamma_{ss} & \Gamma_{sp_2} \\ \Gamma_{p_1 s} & \Gamma_{p_1 p_2} \end{pmatrix} \begin{pmatrix} A_s \\ A_p \end{pmatrix} \times \frac{\vec{a} \cdot \vec{b}}{I_{pump} + I_{sig}}, \quad (4)$$

in which $A_{s,p}$ and $B_{s,p}$ are the amplitudes of the pump and signal beams for the different polarizations. s polarization refers to the case where the electric field vector is perpendicular to the incident plane; for p polarization the polarization vector is parallel to this plane. p_1 refers to the signal beam and p_2 to the pump beam. The intensities of the pump and signal beams I_{pump} and I_{sig} are given by the square of the field amplitudes, e.g., $I_{pump} \sim A_s^2 + A_p^2$. The angular frequency of the laser is denoted by ω ; the beam angle inside the crystal is 2θ , the magnetic susceptibility of the material is denoted by μ , the laser wavelength by λ , and the matrix elements Γ_{ij} represent the coupling between signal and pump beams with their respective polarizations, which are related to the permittivity change [Eq. (3)] by [24]

$$\Gamma_{ij} = n^4 r_{41} \left\langle \vec{i} \left| \begin{pmatrix} 0 & E_z & E_y \\ E_z & 0 & E_x \\ E_y & E_x & 0 \end{pmatrix} \right| \vec{j} \right\rangle, \quad (5)$$

where $\vec{i}, \vec{j} = \vec{p}_1, \vec{p}_2$ or \vec{s} . The scalar product of the polarization vectors of the two beams in the last term in Eq. (4) is given by

$$\vec{a} \cdot \vec{b} = A_s B_s + A_p B_p \cos \theta, \quad (6)$$

with \vec{p} in the incident plane and perpendicular to the z' axis. Actually, the angle θ in semiconductors is very small due to the large refractive index (3.3 for InP and 3.5 for GaAs). We can assume $\cos \theta = 1$, which implies $\vec{p} = \vec{p}_1 = \vec{p}_2$. In this paper we restrict ourselves to either s or p polarization of the beams. Using identities for the physical parameters and for signal intensities much smaller than the pump intensity $I_{sig} \ll I_{pump}$, Eq. (4) can then be further reduced to

$$\frac{\partial B_i}{\partial z'} = \frac{\pi}{\lambda n \cos \theta} \Gamma_{ii} B_i, \quad (7)$$

with $i = s$ or p . The intensity change of the signal beam is given by

$$\frac{\partial I_{sig}}{\partial z'} \sim \frac{\partial B_i^2}{\partial z'} = 2B_i \frac{\partial B_i}{\partial z'} = \frac{2\pi}{\lambda n \cos \theta} \Gamma_{ii} B_i^2. \quad (8)$$

The gain coefficient is obtained from Eq. (1) and Eq. (8) as

$$\Gamma = \frac{1}{B_i^2} \frac{\partial B_i^2}{\partial z'} = \frac{2\pi}{\lambda n \cos \theta} \Gamma_{ii}. \quad (9)$$

The matrix element Γ_{ii} given by Eq. (5) is calculated for a specific orientation of the space charge field \vec{E} and polarization \vec{i} by representing these vectors in the crystallographic system using the three Euler angles Φ , Θ , Ψ (Fig. 2). These angles give the orientation of the laboratory $x'-y'-z'$ system with respect to the crystallographic $x-y-z$ system. The space charge field is in the x' direction, which is in the plane of the two incident beams. The

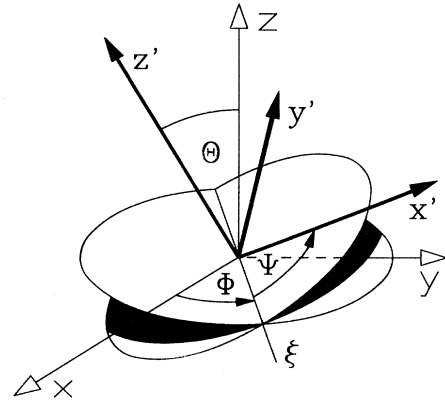


FIG. 2. Definition of Euler angles as used in the text. The electric field vector \vec{E} is in all cases, except for the contradictory geometry (Fig. 11), parallel to the x' axis. The polarization vector \vec{p} is in all cases parallel to the x' axis. The polarization vector \vec{s} is parallel to the y' axis.

z' axis is the bisector of the two incident beams, which is in all cases perpendicular to the crystal surface except in the experiments of Figs. 9 and 11. The angle Ψ describes the rotation of the crystal around the z' axis or surface normal.

The space charge field is given by the vector

$$\vec{E} = (E_x, E_y, E_z) = E_{sc}(\bar{x}, \bar{y}, \bar{z}), \quad (10)$$

where E_{sc} is the amplitude of the space charge field \vec{E} and \bar{x} , \bar{y} , and \bar{z} give its projections on the three crystal axes.

$$\bar{x} = \cos \Phi \cos \Psi - \cos \Theta \sin \Phi \sin \Psi, \quad (11a)$$

$$\bar{y} = \sin \Phi \cos \Psi + \cos \Theta \cos \Phi \sin \Psi, \quad (11b)$$

$$\bar{z} = \sin \Theta \sin \Psi. \quad (11c)$$

In the case of p polarization we have $\vec{E} \parallel \vec{p}$ and

$$\vec{i} = \vec{p} = (\bar{x}, \bar{y}, \bar{z}). \quad (12)$$

With Eq. (10) one obtains from Eq. (5)

$$\Gamma_{pp} = 6n^4 r_{41} E_{sc} \bar{x} \bar{y} \bar{z}. \quad (13)$$

From Eq. (13) it is obvious, that for p polarization the matrix element only depends on the coordinates of the electric field vector $\bar{x}, \bar{y}, \bar{z}$, which can be described by means of two angles Φ, Ψ' in a polar coordinate system with

$$\bar{x} = \cos \Phi \cos \Psi', \quad (14a)$$

$$\bar{y} = \sin \Phi \cos \Psi', \quad (14b)$$

$$\bar{z} = \sin \Psi'. \quad (14c)$$

By comparing these equations with Eqs. (11), it is obvious that the Euler angle Ψ is identical to Ψ' , if $\Theta = 90^\circ$ is chosen. The angular dependence of the gain coefficient is then given by

$$\Gamma_{pp}(\Phi, \Psi') = \frac{3}{4} n^4 r_{41} E_{sc} (\sin \Psi' + \sin 3\Psi') \sin 2\Phi. \quad (15)$$

This orientational dependence of the gain coefficient with respect to the crystal axes is shown in Fig. 3. In the

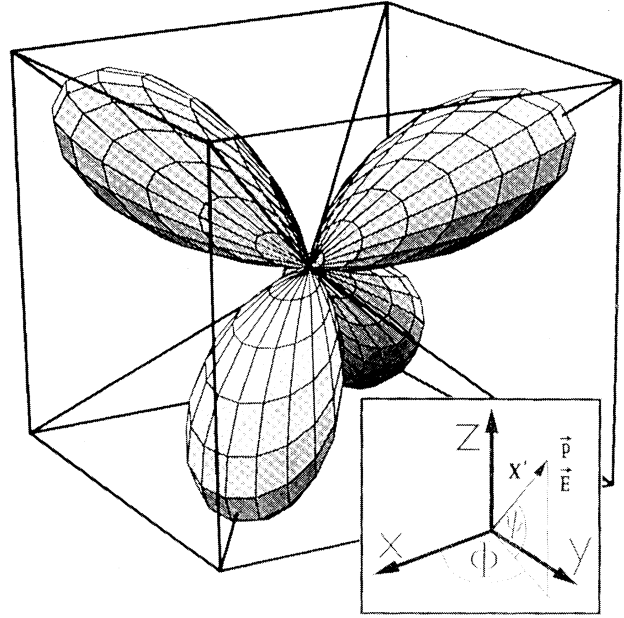


FIG. 3. Matrix element $\Gamma_{pp}(\Phi, \Psi')$ in polar coordinates; the cube represents the crystallographic axes. The inset defines the angles Φ and Ψ (with $\Theta = 90^\circ$) or Ψ' for this and the following figures. The crystallographic (111) and equivalent axes are also shown. The viewpoint is close to the $(\bar{1}\bar{1}\bar{1})$ direction.

case of p polarization this picture represents the general case for all possible sample orientations. For comparison with the experimental data we have chosen r_{41} to be negative, as is the case for the relevant photorefractive semiconductors [17,25,26]. The maximum value of Eq. (15) is obtained analytically as $\Gamma_{pp}^{max} = (2/\sqrt{3})n^4 r_{41} E_{sc}$, if \vec{E} is along the (111) or equivalent axes. This is 15% larger than in the case of s polarization [17].

The expression of Eq. (13) in terms of the three Euler angles from Eqs. (11) is convenient, if misoriented samples with surfaces not parallel to one of the major crystallographic axes, have to be characterized:

$$\Gamma_{pp}(\Phi, \Theta, \Psi) = \frac{3}{4} n^4 r_{41} E_{sc} [\sin \Theta \sin 2\Phi (\sin \Psi + \sin 3\Psi) + \sin 2\Theta \cos 2\Phi (\cos \Psi - \cos 3\Psi) - \frac{1}{4} (\sin \Theta + \sin 3\Theta) \sin 2\Phi (3 \sin \Psi - \sin 3\Psi)]. \quad (16)$$

Equation (16) transforms into Eq. (15) for $\Theta = 90^\circ$ and $\Psi = \Psi'$.

In the case of s polarization we have $\vec{E} \perp \vec{s}$ and $\vec{i} = \vec{s} = (\hat{x}, \hat{y}, \hat{z})$ with

$$\hat{x} = -\cos \Phi \sin \Psi - \cos \Theta \sin \Phi \cos \Psi, \quad (17a)$$

$$\hat{y} = -\sin \Phi \sin \Psi + \cos \Theta \cos \Phi \cos \Psi, \quad (17b)$$

$$\hat{z} = \sin \Theta \cos \Psi, \quad (17c)$$

and one obtains from Eq. (5)

$$\Gamma_{ss}(\Phi, \Theta, \Psi) = 2n^4 r_{41} (E_x \hat{y} \hat{z} + E_y \hat{z} \hat{x} + E_z \hat{x} \hat{y}). \quad (18)$$

In the case of s polarization, all three Euler angles are generally necessary. The angular dependence of the gain coefficient Γ_{ss} is then given by

$$\Gamma_{ss}(\Phi, \Theta, \Psi) = \frac{1}{4}n^4r_{41}E_{sc}[\sin 2\Phi \sin \Theta(\sin \Psi - 3 \sin 3\Psi) + \cos 2\Phi \sin 2\Theta(\cos \Psi + 3 \cos 3\Psi) - \frac{3}{4} \sin 2\Phi(\sin \Theta + \sin 3\Theta)(\sin \Psi + \sin 3\Psi)] . \quad (19)$$

The maximum gain for s polarization is obtained if \vec{E} and \vec{s} are in the (110) planes with $\Gamma_{ss}^{max} = n^4r_{41}E_{sc}$.

For comparison also for s polarization the case $\Theta = 90^\circ$ is given:

$$\Gamma_{ss}(\Phi, \Theta = 90^\circ, \Psi) = \frac{1}{4}n^4r_{41}E_{sc} \sin 2\Phi(\sin \Psi - 3 \sin 3\Psi). \quad (20)$$

In contrast to the case of p polarization where $\Gamma_{pp}(\Phi, \Theta = 90^\circ, \Psi = \pm 90^\circ) = 0$ is uniquely defined, $\Gamma_{ss}(\Phi, \Theta = 90^\circ, \Psi = \pm 90^\circ) = f(\Phi)$ is a multiple function of Φ at the poles of the polar diagram. This discontinuity can be removed by representing Γ_{ss} in terms of a new angle $\hat{\Psi} = \Psi + 90^\circ$. Fig. 4 gives a three dimensional plot of the orientational dependence of the gain coefficient $\Gamma_{ss}(\Phi, \Theta = 90^\circ, \hat{\Psi})$ in polar coordinates. Because of the special choice of Θ Fig. 4 only represents cases, where the plane spanned by the \vec{E} and \vec{s} vectors is parallel to the crystal z axis.

As shown in the inset, the figure shows the magnitude of the gain coefficient in the direction of the polarization vector \vec{s} . For example, the maximum values for s polar-

ization can be obtained in the (110) and $(\bar{1}\bar{1}0)$ planes. The space charge field \vec{E} is in this case antiparallel to the vertical axis, representing $\langle 001 \rangle$ and the polarization vector \vec{s} is parallel to the $\langle 1\bar{1}0 \rangle$ or $\langle 110 \rangle$ directions.

IV. RESULTS AND DISCUSSION

Photorefractive TWM experiments were done on GaAs and InP samples, cut in different crystallographic orientations, i.e., the major crystallographic axes. The Ψ dependence of the gain coefficient was recorded for s - and p polarization. We will first focus the discussion on the results for p polarization.

The angular dependence of the gain coefficient Γ_{pp} for p polarization in an experiment as sketched in Fig. 1 is given by the intersection of the gain-coefficient surface $\Gamma(\Phi, \Psi)$ with the $x'y'$ plane in the laboratory system, which corresponds to the crystal surface plane. This is shown in Fig. 5 for the case of the (110) plane, where $\Phi = -45^\circ$. Figure 6(a) gives the experimental data together with the theoretical expression:

$$\Gamma_{pp}(-45^\circ, 90^\circ, \Psi) = -\frac{3}{4}n^4r_{41}E_{sc}(\sin \Psi + \sin 3\Psi) . \quad (21)$$

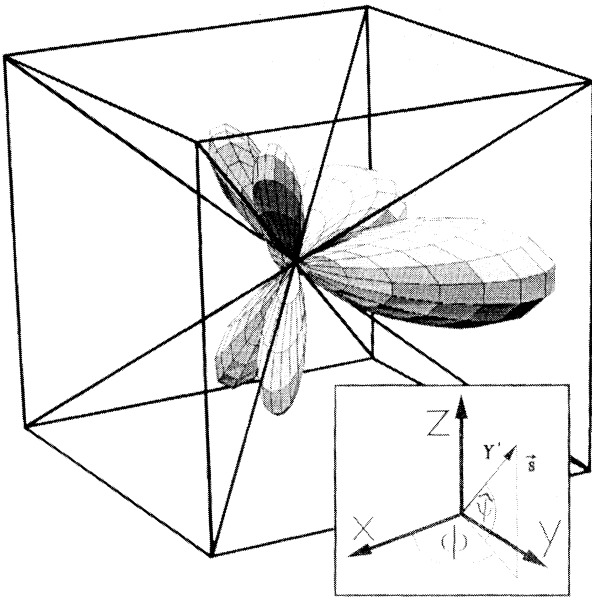


FIG. 4. Magnitude of the matrix element $\Gamma_{ss}(\Phi, \hat{\Psi})$ in polar coordinates with $\Theta = 90^\circ$. The angle $\hat{\Psi}$ is related to the Euler angle by $\hat{\Psi} = \Psi + 90^\circ$. The cube represents the crystallographic axes. The crystallographic $\langle 111 \rangle$ and equivalent axes are also shown.

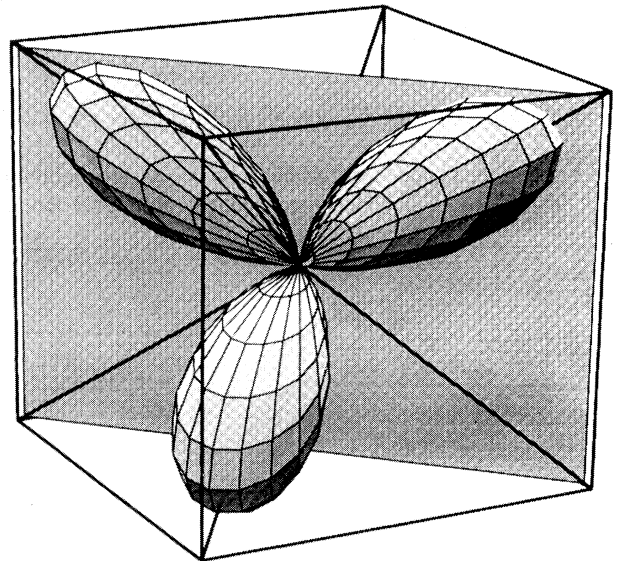


FIG. 5. Construction of the orientational dependence of the gain coefficient Γ_{pp} , if the \vec{E} field is in the (110) plane, by intersection of the three-dimensional gain-coefficient surface $\Gamma_{pp}(\Phi, \Psi')$ with the (110) plane.

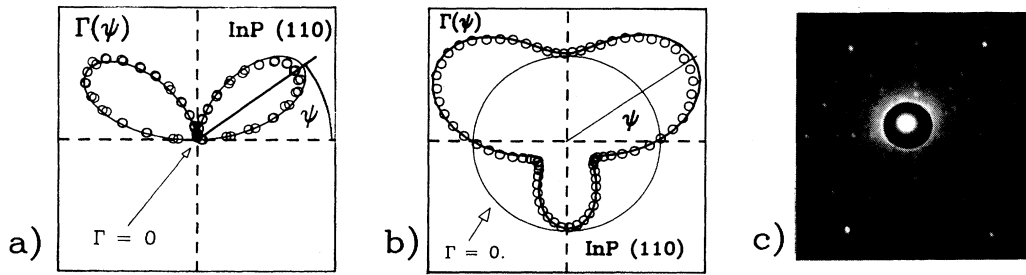


FIG. 6. Experimental gain coefficient $\Gamma(\Psi)$ and theory $\Gamma_{pp}(\Psi)$ according to Eq. (21) for an InP:Fe sample and a (110)-surface. The experimental angle Ψ is defined in the picture; in this case it is positioned to show the direction of the crystal (111) axis. (a) Representation in polar coordinates; $\Gamma^{max} = 0.3 \text{ cm}^{-1}$. (b) Same as (a), but showing the inversion symmetry of the photorefractive effect, by using a polar coordinate system with an off-set. (c) Laue diagram of this surface plane.

As positive and negative gain cannot be distinguished in this representation, we choose a polar coordinate system with an offset, as shown in Fig. 6(b). Also in this representation the inversion symmetry $\Gamma(\Psi) = -\Gamma(\Psi + \pi)$ can be seen and the mirror symmetry at the $(\bar{1}\bar{1}0)$ plane, which is cutting through the vertical line in the diagram, is apparent. Furthermore, the directions of maximum gain are the crystallographic $\langle 111 \rangle$ and $\langle \bar{1}\bar{1}\bar{1} \rangle$ axes, as is expected. A corresponding Laue diagram of the crystal surface confirms this orientation [Fig. 6(c)].

If the incident beam bisector is parallel to the highest symmetry axis $\langle 111 \rangle$, the threefold symmetry of the $\bar{4}3m$ space group is visible and

$$\Gamma_{pp}(45^\circ, -54.7^\circ, \Psi) = -n^4 r_{41} E_{sc} \frac{\sqrt{6}}{3} \sin 3\Psi, \quad (22)$$

where the exact value of the second Euler angle is $\Theta = -\arctan \sqrt{2}$. Figure 7 shows the experimental and calculated data. The calculated Γ_{pp} curve is obtained also by the intersection of the gain-coefficient surface with the (111) plane. The maximal gain here is about 30% smaller than that for the (110) plane.

As Fig. 3 shows, the gain coefficient is zero if \vec{E} is in the (100) plane. This is experimentally verified using a GaAs:Cr sample with a perfect (100) surface, as shown in Fig. 8(a). The corresponding Laue diagram is given in Fig. 8(b). Using a crystal with a slight surface misalignment into the $\langle 111 \rangle$ direction, we observed a clear signal as shown in Figs. 8(c) and 8(d). The data can be fitted by proper choice of angles in Eq. (16). The corresponding theoretical plot in Fig. 8(c) is obtained with $\Phi = -45^\circ$ and $\Theta = 6^\circ$, resulting after some algebraic transformations in Eq. (23):

$$\Gamma_{pp}(-45^\circ, 6^\circ, \Psi) = n^4 r_{41} E_{sc} \left[c_2 \sin^3 \Psi - \frac{c_1}{4} (\sin \Psi + \sin 3\Psi) \right], \quad (23)$$

where $c_1 = 3 \sin 6^\circ$ and $c_2 = c_1 \cos^2 6^\circ$. From the Laue diagram a tilt angle of 5.5° from $\langle 100 \rangle$ on the (110) plane towards $\langle 111 \rangle$ can be deduced; this is in good agreement

with the experimental Γ_{pp} plot in Fig. 8(c).

Using the (100)-oriented sample of Figs. 8(a) and 8(b), a tilt of 45° produces an internal angle of the electrical field \vec{E} with respect to the $\langle 100 \rangle$ axis, as shown in Figs. 9(a) and 9(b). We observed a clear photorefractive signal depicting the additional mirror plane introduced by

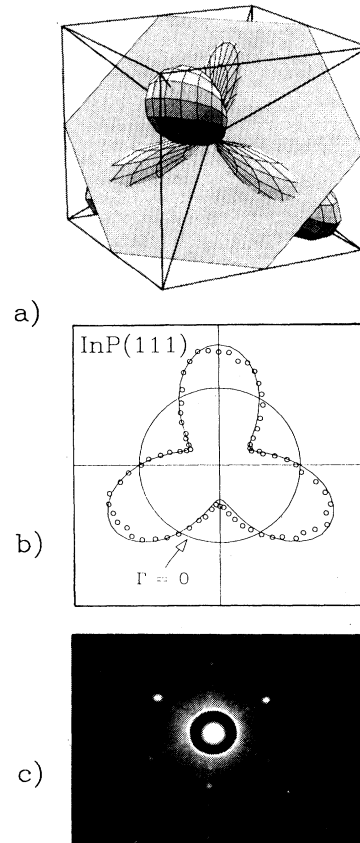


FIG. 7. Experimental gain coefficient $\Gamma(\Psi)$ for InP:Fe and theory $\Gamma_{pp}(\Psi)$ according to Eq. (22) for an InP:Fe sample with a (111)-surface. (a) Intersection of the theoretical gain-coefficient surface $\Gamma_{pp}(\Phi, \Psi')$ with the crystallographic (111) plane. In contrast to Fig. 3 the viewpoint is from the $\langle \bar{1}\bar{1}\bar{1} \rangle$ direction. (b) Experimental data and theoretical curve according to Eq. (22); $\Gamma^{max} = 0.2 \text{ cm}^{-1}$. (c) Laue diagram of this (111)-surface plane.

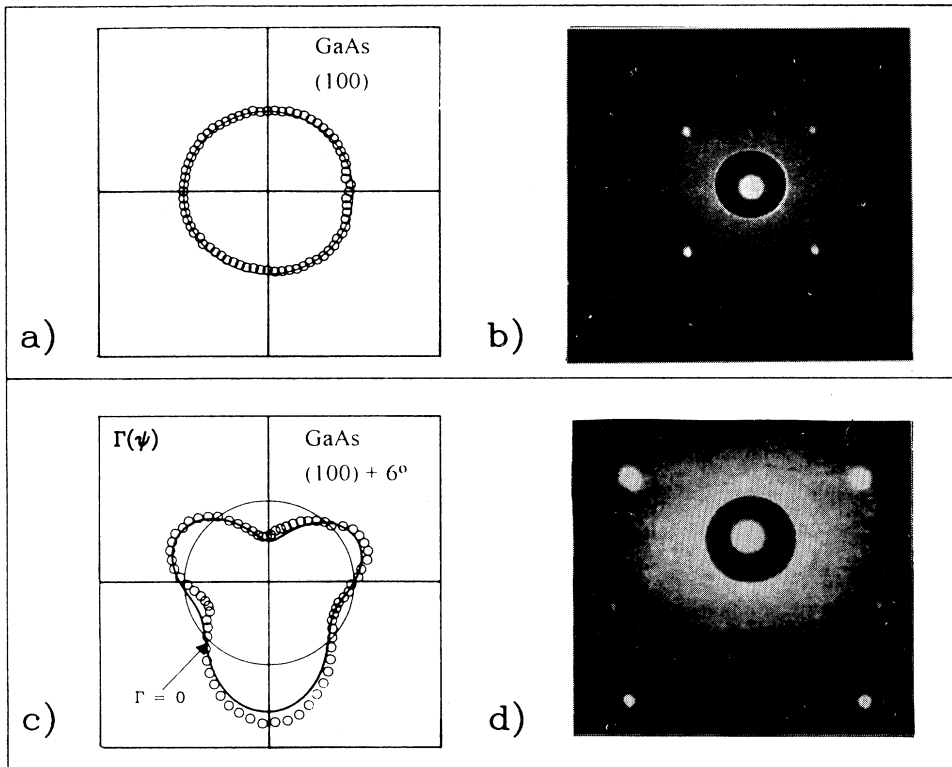


FIG. 8. Experimental gain coefficient $\Gamma(\Psi)$ for (100)-oriented and a misoriented GaAs:Cr wafer. (a) Photorefractive gain coefficient $\Gamma(\Psi)$ for the wafer, exactly oriented in the (100) plane; $\Gamma^{max} = 0 \text{ cm}^{-1}$. (b) Laue diagram of the crystal with the (100) plane. (c) Photorefractive gain coefficient of a GaAs:Cr crystal, with surface misoriented at 6° in (110) towards $\langle 111 \rangle$. The solid line represents the theory as outlined in the text, according to Eq. (23); $\Gamma^{max} = 0.13 \text{ cm}^{-1}$. (d) Laue diagram of the crystal of (c).

this experimental setup. In this case the electrical field \vec{E} performs a rotation on a conical surface, which again produces maximum gain, if oriented close to $\langle 111 \rangle$. To a first approximation, this is similar to the orientational dependence of the case of Fig. 8(c). However, a detailed quantitative analysis requires tracing of the two beams, whose polarizations are no longer parallel inside of the sample, and evaluation of the four matrix elements of Eq. (4), which are not given at this point. Instead, we want to stress the possibility of achieving a sizable photorefractive effect for commercial (100)-oriented wafers

by this method. This was applied in the past for the determination of doping profiles [8].

The expected gain for nonoptimal orientations can be calculated by changing the direction of \vec{E} from the $\langle 100 \rangle$ axis with $\Gamma = 0$ to the $\langle 111 \rangle$ axis with $\Gamma = \Gamma_{max}$. As can be seen from the three-dimensional representations in Fig. 3, the gain coefficient Γ is a rapidly increasing function of the angle Ψ from $\langle 100 \rangle$. The theoretical plot according to Eq. (21) is shown in Fig. 10. Already 50%

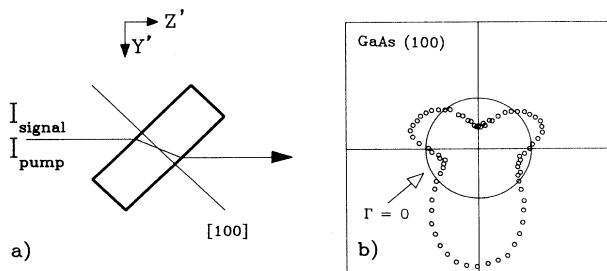


FIG. 9. Experimental arrangement for observing photorefractive gain from the crystal with the exact (100) surface used in Figs. 8(a) and 8(b). (a) Experimental setup with a tilted sample. (b) Photorefractive gain coefficient $\Gamma(\Psi)$, as obtained for a (100) GaAs crystal with the setup of (a). $\Gamma^{max} = 0.06 \text{ cm}^{-1}$.

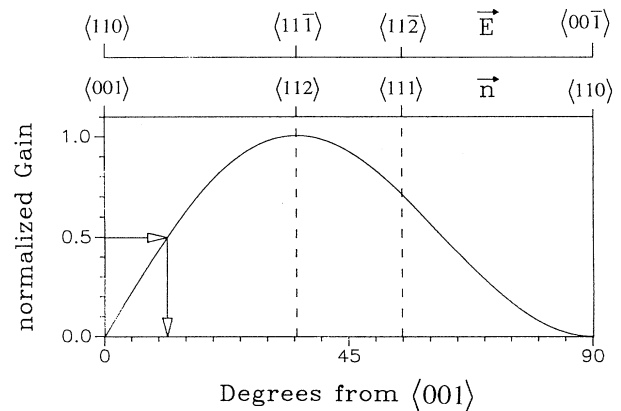


FIG. 10. Dependence of the gain coefficient Γ on the misalignment from the $\langle 001 \rangle$ axis. \vec{n} represents the surface normal. Already 50% of the maximum gain is obtained at an angle of 12° of the \vec{E} field inside the crystal.

of the maximum gain can be observed at only 12° from the $\langle 100 \rangle$ axis.

An experiment in the contradirectional geometry, shown in Fig. 11(a), also produces gain for $\langle 100 \rangle$ -oriented crystals. In this case the electric field vector is constant and along the crystal z axis, resulting in an angular dependence which is directly calculated from Eq. (5),

$$\Gamma_{pp}(\Psi) = n^4 r_{41} E_{sc} \sin 2\Psi. \quad (24)$$

Figure 11(b) shows the fourfold symmetry with respect to rotations around the $\langle 100 \rangle$ axis, the Laue diagram of Fig. 8(b). As the \vec{E} vector has constant direction in this case along the x , respectively, z' axis, the additional mirror planes (011) and $(0\bar{1}\bar{1})$ can be observed. They are positioned at $\pm 45^\circ$ in the diagram.

However, in the contradirectional geometry the obtainable range of fringe spacings lies between 0.16 and 0.18 μm only, much lower than the optimal grating spacing of 1 μm in our samples, leading to a reduction of the absolute gain.

In Figs. 12(a)–12(d) we present the experimental results and theoretical fits on differently oriented crystals for s polarization. The theoretical fits to the experimental data were obtained using the amplitude ratio between s and p data as given by the theory, thereby fitting s and p data simultaneously. These figures should be compared with the corresponding data and theory for p polarization.

Figure 12(a) depicts the orientational dependence in the $\langle 100 \rangle$ plane in the contradirectional geometry. The resulting equation is

$$\Gamma_{ss}(\Psi) = -n^4 r_{41} E_{sc} \sin 2\Psi. \quad (25)$$

Because the \vec{E} vector is constant in this case, the s polarized signal wave is probing the identical, constant index ellipsoid as in the case of p polarization. The resulting angular dependence is identical to Eq. (24), but rotated by the 90° angle between the \vec{s} and \vec{p} vectors.

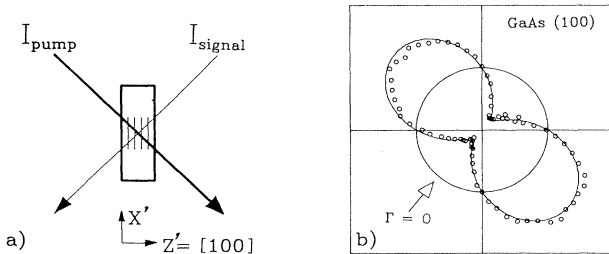


FIG. 11. Experimental arrangement for observing photorefractive gain from the crystal with the exact $\langle 100 \rangle$ surface used in Figs. 8(a) and 8(b) in the contradirectional geometry. (a) Schematic of experimental setup. (b) Photorefractive gain coefficient $\Gamma(\Psi)$ for the same crystal. The solid line represents the theory according to Eq. (23) with $\Gamma^{max} = 0.11 \text{ cm}^{-1}$.

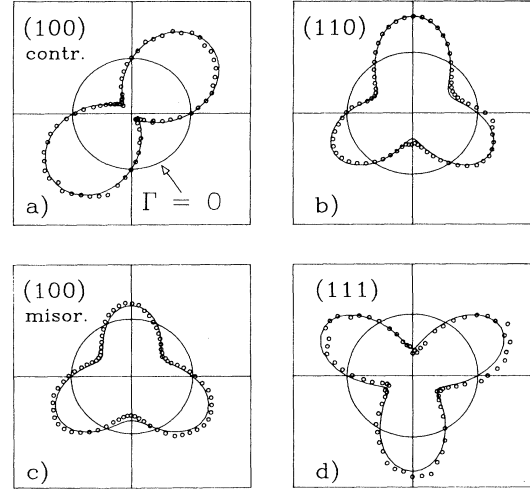


FIG. 12. Experimental data and theoretical fit for s polarization and the samples of Figs. 6–9, and 11, (a) GaAs:Cr sample with a $\langle 100 \rangle$ surface in the arrangement of Fig. 11; $\Gamma^{max} = 0.11 \text{ cm}^{-1}$. (b) InP:Fe sample with a $\langle 110 \rangle$ surface, the same as used for Fig. 6; $\Gamma^{max} = 0.25 \text{ cm}^{-1}$. (c) GaAs:Cr misoriented sample, the same as used in Figs. 8(c) and 8(d); $\Gamma^{max} = 0.08 \text{ cm}^{-1}$. (d) InP:Fe sample with a $\langle 111 \rangle$ surface, the same as used in Fig. 7; $\Gamma^{max} = 0.2 \text{ cm}^{-1}$.

Figures 12(b)–12(d) are in the usual, forward geometry of Fig. 1. Figure 12(b) shows the Ψ dependence of the gain in the $\langle 110 \rangle$ plane. The resulting equation is

$$\Gamma_{ss}(-45^\circ, 90^\circ, \Psi) = -\frac{1}{4} n^4 r_{41} E_{sc} (\sin \Psi - 3 \sin 3\Psi). \quad (26)$$

Figure 12(c) shows the case of the 6° misoriented sample of Figs. 8(c) and 8(d). The equation for s polarization is given by

$$\Gamma_{ss}(-45^\circ, 6^\circ, \Psi) = -\frac{1}{4} n^4 r_{41} E_{sc} \times \left[\frac{c_1}{6} (\sin \Psi + 3 \sin 3\Psi) - \frac{c_3}{4} (\sin \Psi + 3 \sin 3\Psi) \right], \quad (27)$$

where c_1 is given in Eq. (23) and $c_3 = 3 \sin^3 6^\circ$. The maximum gain is only 60% compared to the case of p polarization.

Finally, the threefold symmetry of the $\langle 111 \rangle$ plane is apparent in Fig. 12(d). The associated equation is

$$\Gamma_{ss}(45^\circ, -54.7^\circ, \Psi) = n^4 r_{41} E_{sc} \frac{\sqrt{6}}{3} \sin 3\Psi. \quad (28)$$

This result is, except for the sign, identical to the case of p polarization, as given by Eq. (22) and shown in

Fig. 7. This is the only case for s polarization where the matrix element Γ_{ss} does not depend explicitly on the direction of the polarization vector \vec{s} but is solely a function of the direction of the space charge field \vec{E} .

V. CONCLUSIONS

We have evaluated the photorefractive gain coefficient for general spatial orientation of samples belonging to the $\bar{4}3m$ space group. Experiments with differently cut samples confirm the theoretical analysis. Commercial wafers cut in the (100) plane can be used with 50% of the max-

imum gain under suitable experimental conditions. This opens the possibility of a contactless determination of material parameters connected to the photorefractive effect such as crystal orientation, concentration of deep levels, conductivity, etc.

ACKNOWLEDGMENTS

This work was supported by the Bundesministerium für Forschung und Technologie and VDI-Technologiezentrum of Germany.

-
- [1] M. B. Klein, *Opt. Lett.* **9**, 350 (1984).
 - [2] A. M. Glass, A. M. Johnson, D. H. Olson, W. Simpson, and K. A. Ballmann, *Appl. Phys. Lett.* **44**, 948 (1984).
 - [3] R. B. Bylsma, P. M. Bridenbaugh, D. H. Olson, and A. M. Glass, *Appl. Phys. Lett.* **51**, 889 (1987).
 - [4] L. J. Cheng, G. Gheen, M. F. Rau, and F. C. Wang, *J. Appl. Phys.* **62**, 3991 (1987).
 - [5] G. Gheen and L. J. Cheng, *Appl. Phys. Lett.* **51**, 1481 (1987).
 - [6] A. E. Chiou and P. Yeh, *Opt. Lett.* **11**, 461 (1986).
 - [7] T. Y. Chang, *Opt. Lett.* **15**, 461 (1990).
 - [8] R. B. Bylsma, D. H. Olson, and A. M. Glass, *Appl. Phys. Lett.* **52**, 1083 (1988).
 - [9] A. M. Glass, M. B. Klein, and G. C. Valley, *Electron. Lett.* **21**, 221 (1985).
 - [10] B. Imbert, H. Rajbenbach, S. Mallick, J. P. Herriau, and J. P. Huignard, *Opt. Lett.* **13**, 327 (1988).
 - [11] G. Picoli, P. Gravey, C. Ozkul, and V. Vieux, *J. Appl. Phys.* **66**, 3798 (1989).
 - [12] H. J. Eichler, Y. Ding, and B. Smandek, *Opt. Commun.* **94**, 127 (1992).
 - [13] H. Rajbenbach, B. Imbert, J. P. Huignard, and S. Mallick, *Opt. Lett.* **14**, 78 (1989).
 - [14] V. Vieux, P. Gravey, N. Wolffer, and G. Picoli, *Appl. Phys. Lett.* **58**, 2880 (1991).
 - [15] P. Yeh, *J. Opt. Soc. Am. B* **4**, 1382 (1987).
 - [16] K. Walsh, T. J. Hall, and R. Burge, *Opt. Lett.* **12**, 1026 (1987).
 - [17] J. Strait, J. D. Reed, and N. V. Kukhtarev, *Opt. Lett.* **15**, 209 (1990).
 - [18] J. C. Fabre, J. M. C. Jonathan, and G. Rosen, *Opt. Commun.* **65**, 257 (1988).
 - [19] G. Khitrova, D. Roueda, N. V. Kukhtarev, and H. M. Gibbs, *Phys. Rev. Lett.* **62**, 1110 (1989); I. Stepanov, *ibid.* **65**, 935 (1990); G. Khitrova *et al.*, *ibid.* **65**, 936 (1990).
 - [20] S. I. Stepanov, S. M. Shandarov, and N. D. Khatkov, *Fiz. Tverd. Tela (Leningrad)* **29**, 3054 (1987) [*Sov. Phys. Solid State* **29**, 1754 (1987)].
 - [21] G. Pauliat, P. Mathey, and G. Roosen, *J. Opt. Soc. Am. B* **8**, 1942 (1991).
 - [22] P. Günter and M. Zgonik, *Opt. Lett.* **16**, 1826 (1991).
 - [23] S. Haussühl, *Kristallphysik* (Physik Verlag, Weinheim, 1983).
 - [24] P. Yeh, *IEEE J. Quantum Electron.* **QE-25**, 484 (1989).
 - [25] I. P. Kaminow and E. H. Turner, *Proc. IEEE* **54**, 1374 (1966).
 - [26] K. Tata and N. Suzuki, *Jpn. J. Appl. Phys.* **19**, 2295 (1980).

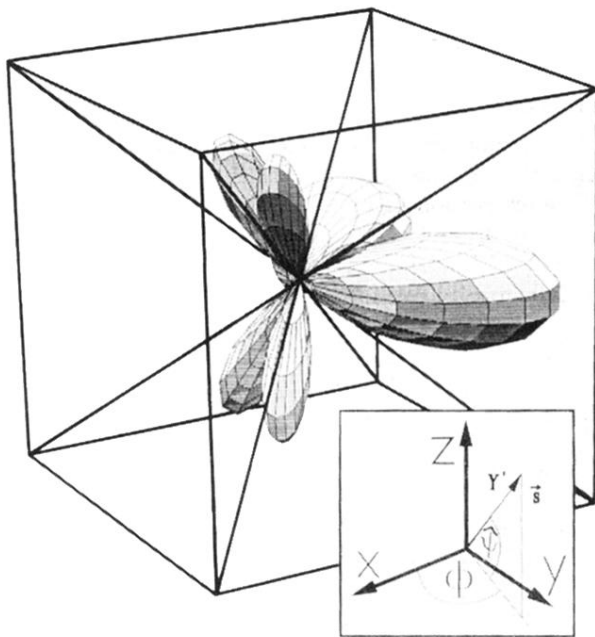


FIG. 4. Magnitude of the matrix element $\Gamma_{ss}(\Phi, \hat{\Psi})$ in polar coordinates with $\Theta = 90^\circ$. The angle $\hat{\Psi}$ is related to the Euler angle by $\hat{\Psi} = \Psi + 90^\circ$. The cube represents the crystallographic axes. The crystallographic $\langle 111 \rangle$ and equivalent axes are also shown.

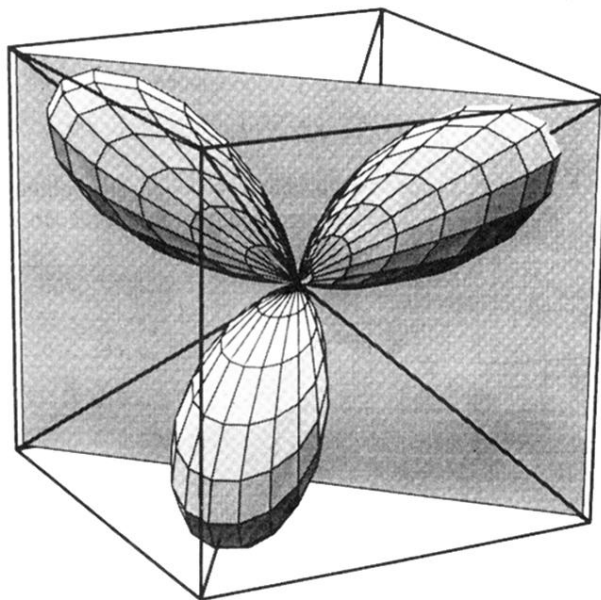


FIG. 5. Construction of the orientational dependence of the gain coefficient Γ_{pp} , if the \vec{E} field is in the (110) plane, by intersection of the three-dimensional gain-coefficient surface $\Gamma_{pp}(\Phi, \Psi')$ with the (110) plane.

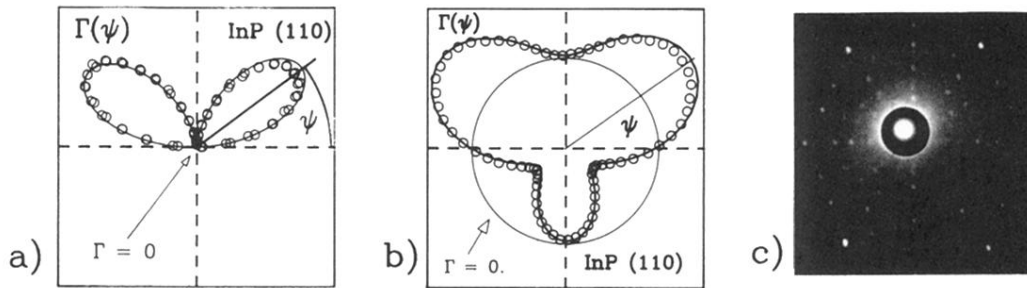


FIG. 6. Experimental gain coefficient $\Gamma(\Psi)$ and theory $\Gamma_{pp}(\Psi)$ according to Eq. (21) for an InP:Fe sample and a (110)-surface. The experimental angle Ψ is defined in the picture; in this case it is positioned to show the direction of the crystal (111) axis. (a) Representation in polar coordinates; $\Gamma^{max} = 0.3 \text{ cm}^{-1}$. (b) Same as (a), but showing the inversion symmetry of the photorefractive effect, by using a polar coordinate system with an off-set. (c) Laue diagram of this surface plane.

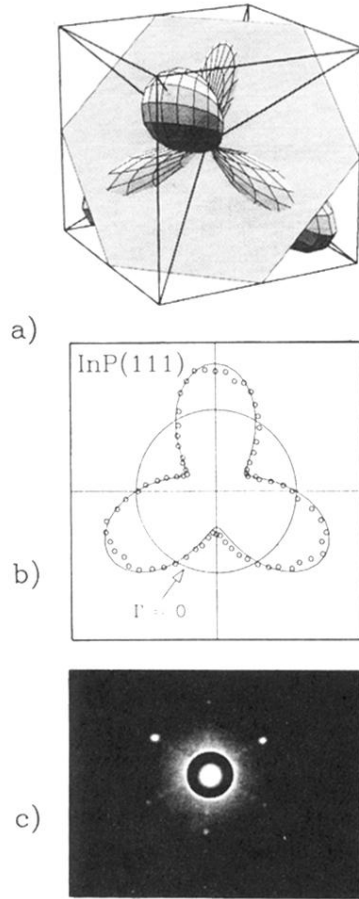


FIG. 7. Experimental gain coefficient $\Gamma(\Psi)$ for InP:Fe and theory $\Gamma_{pp}(\Psi)$ according to Eq. (22) for an InP:Fe sample with a (111)-surface. (a) Intersection of the theoretical gain-coefficient surface $\Gamma_{pp}(\Phi, \Psi')$ with the crystallographic (111) plane. In contrast to Fig. 3 the viewpoint is from the $\langle \bar{1}\bar{1}\bar{1} \rangle$ direction. (b) Experimental data and theoretical curve according to Eq. (22); $\Gamma^{max} = 0.2 \text{ cm}^{-1}$. (c) Laue diagram of this (111)-surface plane.

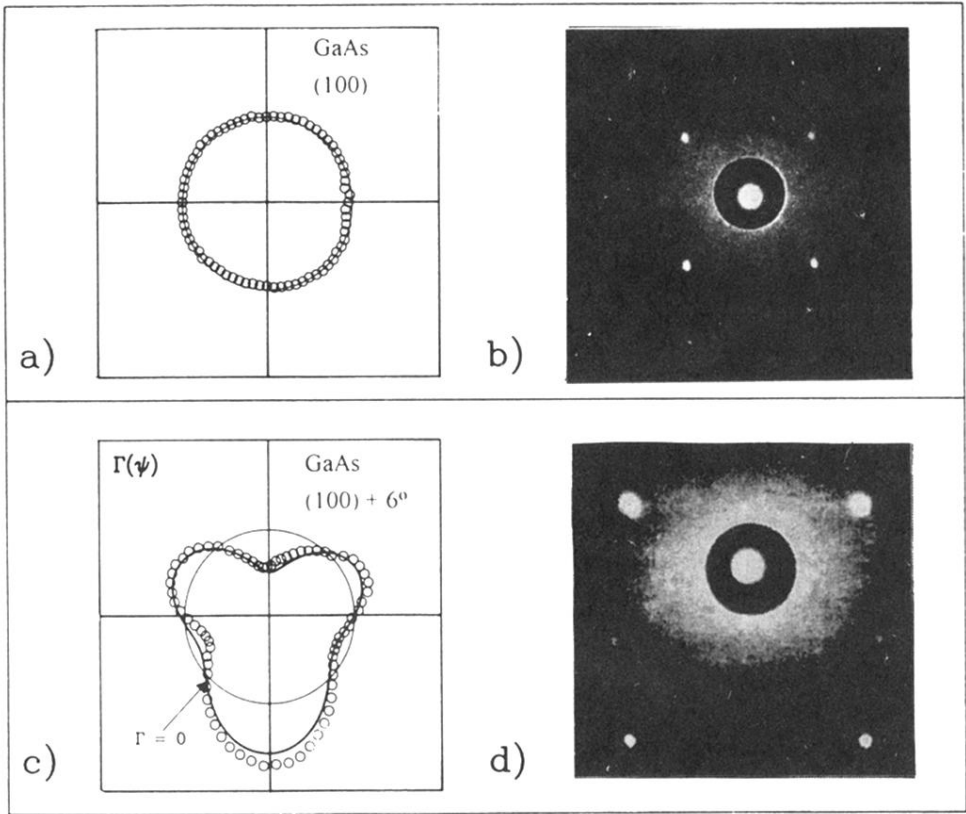


FIG. 8. Experimental gain coefficient $\Gamma(\Psi)$ for (100)-oriented and a misoriented GaAs:Cr wafer. (a) Photorefractive gain coefficient $\Gamma(\Psi)$ for the wafer, exactly oriented in the (100) plane; $\Gamma^{max} = 0 \text{ cm}^{-1}$. (b) Laue diagram of the crystal with the (100) plane. (c) Photorefractive gain coefficient of a GaAs:Cr crystal, with surface misoriented at 6° in (110) towards $\langle 111 \rangle$. The solid line represents the theory as outlined in the text, according to Eq. (23); $\Gamma^{max} = 0.13 \text{ cm}^{-1}$. (d) Laue diagram of the crystal of (c).